Influence of particle entrainment from bed on the powder-snow avalanche dynamics

Christophe Ancey

Cemagref, unité Erosion Torrentielle, Neige et Avalanches, Domaine Universitaire, 38402 Saint-Martin-d'Hères Cedex, France

Abstract. Kulikovskiy and Sveshikova (1977), then Beghin (1981–92) have suggested modelling powder-snow avalanches as buoyant clouds of semi-elliptic shape. Different versions of the equations of motion describing the cloud motion have been put forth by these authors and, subsequently, other researchers. In the last version of his model, Beghin took snow entrainment into account by assuming that all the newly fallen snow can be incorporated into the cloud as a result of the erosive action of the front. The present article examines the reliability of this treatment by considering laboratory experiments and a case study. Laboratory experiments were carried out in order to better understand how an unsteady turbulent gravity current entrains particles from the bed. Comparing observations obtained with density and turbidity currents reveals different entrainment mechanisms. Beghin's model has been applied to the Sionne site (Switzerland), in which a number of powder snow avalanches have been monitored. Comparison of numerical and field data shows a very good agreement as regards the velocity front. In contrast, the model fails to provide the correct order of magnitude for the impact pressure.

1 Introduction

A number of gravity-driven flows are in the form of a particle cloud descending a slope. Typical examples include powder-snow avalanche in mountainous areas and pyroclastic flows from volcanoes; since most natural rapid mass movements of materials can lead to the development of an airborne of particles made up of particle in suspension in the air, dense flows can also sometimes transform into a particle cloud. Evans (1983) reported the case of a rockfall, in which the particle abrasion and fluidization was so intense than a large part of its mass transformed into an airborne. Particle clouds present many similarities with turbidity currents in the ocean as regards their basic flow mechanisms: in both cases, they involve a dilute suspension of small solid particles within the same fluid as the surrounding fluid and the driving force is supplied by the density difference $\Delta\bar{\varrho}$ between the cloud and the surrounding fluid. There is, however, a significant difference between atmospheric and marine clouds: the former are clearly non-Boussinesq flows while for the latter, the Boussinesq approximation holds since the ratio $\Delta\bar{\varrho}/\varrho_a$ is close to unity.

Another difference lies in the boundary conditions of the flows: for turbidity currents, the slope of the continental shelf over they flow is gently inclined (typically a few degrees), the buoyancy supply is regular, and the front velocity is weakly dependent on the slope so that turbidity currents may be seen, at least in a first approximation, as steady currents. In contrast, for particle clouds down mountain slopes, the ground inclination is much more pronounced (typically in the range 15–45°), a finite volume of material is involved in the release, and the front velocity is slope-dependent so that flow is mainly unsteady. As shown by Britter and Linden (1980), bed slope has a significant effect on the entrainment of the surrounding fluid into the current and, thus, the current shape: for gentle slopes, the current takes the form of a head slightly deeper than the following tail while for mild and large slopes, it looks like a semi-elliptic cloud.

Gravity currents can entrain sediment from the bed. For marine turbidity currents involving silts and sand, Parker *et al.* (1986) have shown that a condition for significant erosion and damage potential is that the current reaches a sufficiently high velocity and entrains sediments from the bed. Taking benefit from the steady flow conditions, Parker (1982) and Parker *et al.* (1986) demonstrated that there must be a balance in sediment entrainment and deposition for turbulence not to die in the current. The unsteady character and the non-Boussinesq feature of aerial clouds preclude one to apply the idea developed by Parker to powder-snow avalanches directly. There is some field evidence that snow entrainment from the snowcover plays a key role in the avalanche dynamics. If we admit, as a first approximation, that the leading edge velocity is of dam-break type, that is of the form $u_f = \sqrt{g'h_0}$, where $g' = g\Delta\bar{\varrho}/\varrho_a$ is the reduced gravity and h_0 is the front depth. Typically, field observations provide $h_0 = O(20)$ m and $u_f = O(60)$ m, thus we must have $\Delta\rho/\rho_a = O(20)$. This means that there must be a significant snow entrainment to balance the dilution resulting from the air entrainment. The objective of the article is to examine this point more accurately.

Various approaches to modelling powder-snow avalanches have been proposed over the last thirty years. Soviet researchers can be credited with the first powder snow avalanche models in the 1970s [see Bozhinkiy & Losev (1998)]. At the same period, Tochon-Danguy and Hopfinger (1974) proposed a model inspired from Ellison and Turner's (1959) work on steady plume. However, it was quickly recognized that powder snow avalanches are closer to finite-length, unsteady currents than steady density currents with constant buoyancy supply [Hopfinger & Tochon-Danguy

1977]. This led researchers to treat the problem differently. Kulikovskiy and Sveshikova (1977) set forth a fairly simple model (KS model), in which the cloud was assimilated to a semi-elliptic body whose volume varies with time. The kinematics was entirely described by the mass center position and two geometric parameters of the cloud (the two semi-axes of the ellipse). The cloud density could vary depending on air and snow entrainments. Kulikovskiy and Sveshikova obtained a set of four equations describing the mass, volume, momentum, and turbulent kinetic energy balances. The idea was subsequently redeveloped by Beghin *et al.* (1981), Fukushima et Parker (1986), Akiyama (1999), etc. During his thesis, Beghin developed a model inspired from Escudier and Maxworthy's (1973) study on turbulent thermal formation and very close to the KS model. His first model, presented in an article with Hopfinger and Britter (1981), focused on Boussinesq clouds and ignored particle entrainment, sedimentation, and basal friction. Later on, he extended his former model by dealing with the more realistic case of non-Boussinesq clouds, with varying supply in materials due to sedimentation or entrainment from the bed. The chief difference between KS and Beghin's model is that Kulikovskiy and Sveshikova considered a fourth equation (turbulent kinetic balance equation) while energetic aspects were ignored in Beghin's treatment. Subsequently, Fukushima and Parker (1990) mixed the ideas developed in their former article on steady turbidity current (1986) and the simple geometric treatment contained in the KS model.

At the end of the eighties, a new generation of powder snow avalanche has appeared [Scheiwiller & Hutter (1987); Hermann (1993); Naaim & Gurer (1997); Issler (1998); see also Hutter (1996)]. They rely on the numerical resolution of local equations of motion, including a two-phase mixture approximation and closure equations (usually a $k-\epsilon$ model for turbulence). Though they are undoubtedly a promising approach to modelling powder snow avalanche, their level of sophistication contrasts with the crudeness of their basic assumptions as regards the momentum exchanges between phases, turbulence modification due to the disperse phase, and so on. At this level of our knowledge of physical and natural processes, it is of great interest to still use simple models and to completely explore what they can describe and explain. The viewpoint expressed here does not differ from the philosophy of the Cambridge school of geophysics, which has explored in detail the box-model approximation of turbidity currents [Huppert 1998].

The article examines the effect of snow entrainment in Beghin's model. We will first begin by presenting the basic knowledge of erosion mechanisms occurring in an erodible bed, over which a rapid turbulent current arrives. We will then present how the snow entrainment is accounted for in Beghin's model. The last part of the article is devoted to a case study (comparison with avalanche data obtained in the Sionne site).

2 Snow entrainment from the snow cover

The entrainment of particles from a loose or cohesive particle bed by a turbulent current is an old problem, which has received considerable attention from the end of the XIX$^{\text{th}}$ century, notably in the context of hydraulics (bed load transport in rivers) and in chemical engineering (removal of colloidal particles from substrates). The reader is referred to the work of Garcia and Parker (1997, 1990, 1992) for applications in the context of turbidity currents. Most of the time, steady conditions inside the turbulent current are assumed in order to measure or compute the threshold of incipient motion and the entrainment rate of particles from the bed. Since for fine particles, the turbulence structure depends a great deal on the time equilibrium between the diffusion, advection, production, and dissipation process and thus strongly affects particle entrainment and stratification, the abundant literature on the entrainment-deposition problem is not of great help in our case.

More recently, specific studies have been performed to evaluate the influence of bed load transport on the motion of a water surge. Capart and Young (1998) and Capart and Fraccarollo (2002) have studied the dam break problem for a mobile bed (made up of coarse particles) experimentally and numerically. The authors have shown that an intense entrainment of particles occurs in the snout, leading to a sudden and quasi instantaneous scouring of the bed: particles were lifted up and filled all the wave front, which was much steeper than that observed for a rigid bed. As shown in Fig. 1, the front plays the key role in the particle entrainment.

Beghin performed a series of laboratory experiments to obtain a qualitative picture of entrainment [unpublished work]. For this purpose, he used Hopfinger and Tochon-Danguy's (1977) assumption, stating that it is possible to use Boussinesq flows to simulate powder-snow avalanches in the laboratory, and he further assumed that a powder snow avalanche can be assimilated to a buoyant cloud, that is, a finite-size current. His experiments involved releasing a given amount of heavy fluid contained in a box onto a horizontal plane immersed in a light fluid. A thick film of heady fluid was also deposited along the plane. Using different colored

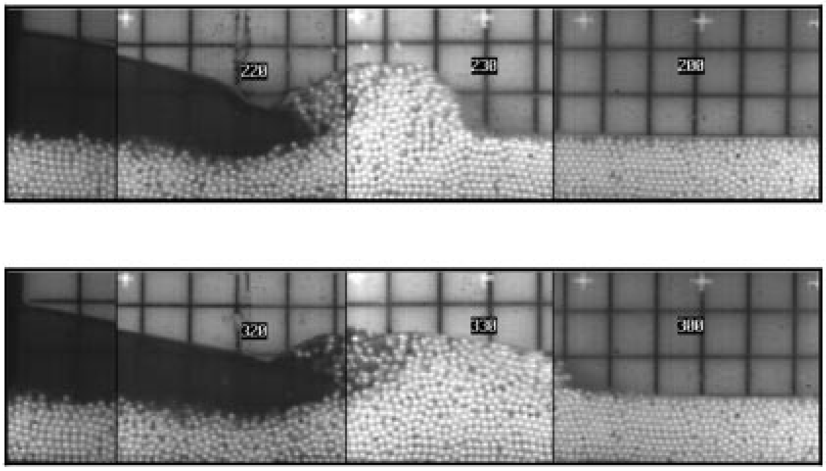

Fig. 1. Image mosaics for the Taipei erosional dam-break wave experiments, conducted with light granular material ($\rho_s = 1048$ kg/m^3). Digital footage from the experiments of Capart & Young (1998). Courtesy of Dr. H. Capart.

brine solutions as heavy fluids made it possible to visualize the entrainment from the ground. As shown in Fig. 2, the fluid at rest is lifted up by the frontal eddy, whose sense of circulation is counter clockwise when the current moves from left to right. The entrained fluid is then incorporated into the current by a series of vortices, which may result from a Kelvin-Helmholtz-like instability [Britter & Simpson 1978]. The entrainment pattern visualized by Beghin did not differ from the one obtained by Hopfinger and Tochon-Danguy (1977) for steady gravity currents.

Further experiments were carried out in the Cemagref by Beghin till 1992, then by Revol, Fehrenbach, Magnard, Clément, and myself, to examine what happens when the heavy fluid is replaced by a suspension and the horizontal plane is replaced by a tilted channel. Such experiments in the laboratory are difficult to run. We had to find a compromise between the "easiness" with which the sediment can be entrained into the cloud and the capacity of the sediment (at rest) to lay over inclined planes without sliding. This problem of selecting a good material is increased by the constraints imposed by similarity conditions. For the sediment to be entrained and maintain in suspension, we have to use light materials, whose settling velocity is low compared to the characteristic velocity of large eddies; this can be achieved by using materials (i) whose density ϱ_s does not differ too much from the density ϱ_a of the surrounding fluid or (ii) whose diameter is very low. In the preliminary tests made with

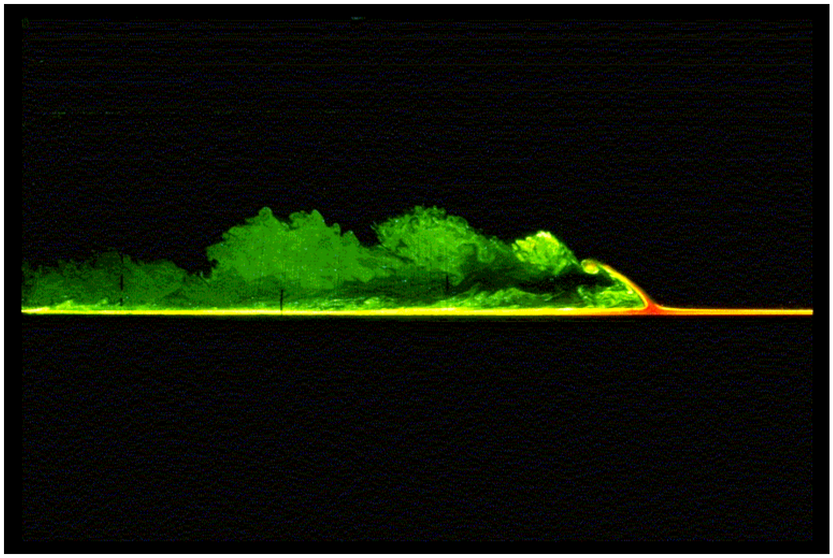

Fig. 2. Entrainment of a colored brine film.

the air as the surrounding fluid, we used kaolin particles. We observed very large velocities of the particle cloud together with a rapid collapse of the cloud. The kaolin particles were likely to quickly aggregate due to electrostatic effects and settled. This led us to use water as the interstitial fluid though it made it impossible to study non-Boussinesq suspensions. We used either sawdust (mean typical diameter $d = 500$ μm, $\varrho_s = 1060$ kg/m^3) or glass beads (mean typical diameter $d = 90\,\mu$m, $\varrho_s = 2450$ kg/m^3). If these materials had very low settling velocities (in the range 6–8 mm/s), they also presented the disadvantage to acquire a cohesion when they were wet. Another experimental problem was that the angle of repose of these materials fell in the range of plane inclinations (typically the range 30–45°); thus, depending on the channel slope, the mobile bed either was very difficult to set in motion or spontaneously slide before the cloud was released. For the particles constituting the erodible bed not to slip along the plane, we covered the plane with a (oscillating or fixed) grid. We observed that the particle cloud was composed of two evident eddies (see Figs 3–4) in agreement with Simpson's (1972) observations. When the cloud moved from left to right, we observed a small vortex ahead the front, whose sense of circulation was clockwise, and a large eddy occupying most of the cloud volume and whose sense of circulation was counter clockwise. The large eddy had a double role: it entrained the surrounding fluid but also the particles from the bed. Indeed, when the cloud moved over the erodible bed, particles were set in motion and formed a dense layer, whose velocity was smaller than the cloud velocity. The large eddy accelerated a part of this dense layer lagging behind the cloud. In this way, particles were entrained from behind.

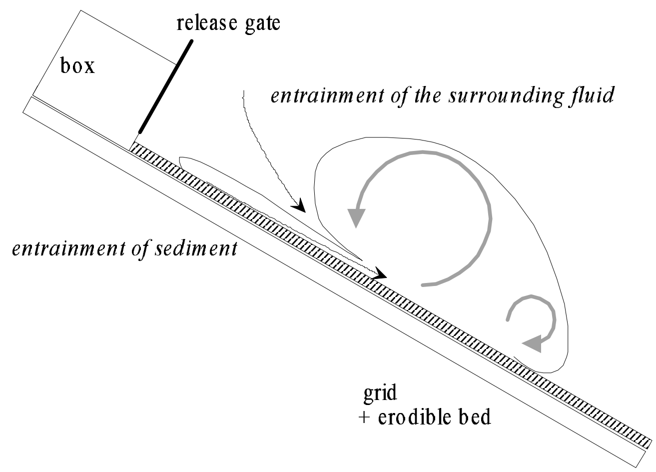

Fig. 3. Sketch of the cloud structure.

In short, the few experiments performed to gain insight into the mechanisms of particle entrainment from the bed shows a complicated pattern. In the experiments made by Capart along with the former experiments of Beghin, the particles were entrained from above into the cloud by the frontal eddy while in our last experiments, they are entrained from the tail.

3 Beghin's model

3.1 Equations of motion and analytical solutions

Beghin's (1981, 1983, 1985, 1990, 1991) model is based on mass and momentum balance equations. Here we focus our attention to purely two-dimensional clouds over an infinite plane. Figure 5 depicts a typical cloud entraining snow from the bed. In the following, h denotes the cloud height, L its length, m its mass, V its volume. The plane inclination with respect to the horizontal is θ. The center of mass of the cloud is located at the abscissa x; its velocity is U. The front position is given by the abscissa

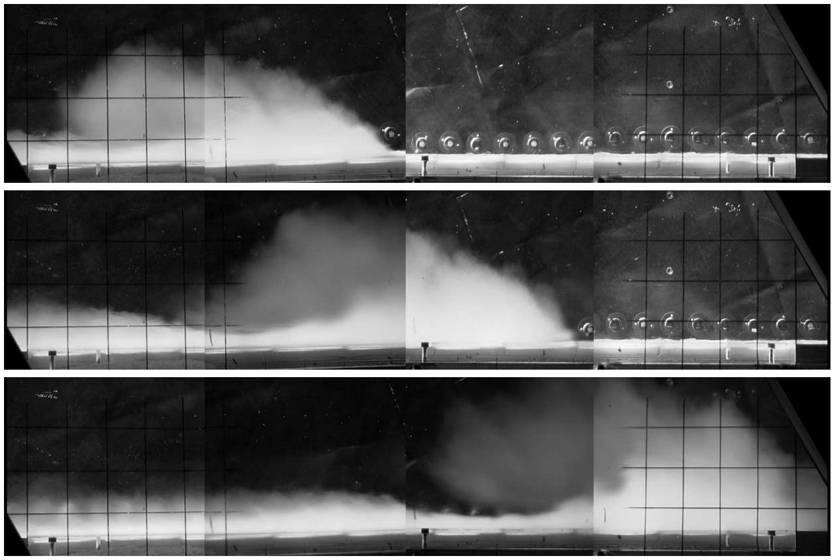

Fig. 4. Series of three photographs showing the motion of the cloud and the particle entrainment.

x_f while its velocity is U_f. The volume solid concentration is ϕ and it is assumed that the cloud is a homogeneous suspension of snow particles of density ϱ_s (no density stratification) in the air (density ϱ_a). The cloud density is then: $\bar{\varrho} = \phi\varrho_s + (1-\phi)\varrho_a$. The surface area (per unit width) exposed to the surrounding fluid is denoted S and can be related to h and L in this way: $S = k_s\sqrt{hL}$, where k_s is a shape factor. Here we assume that the cloud keeps a semi-elliptic form, whose aspect ratio $k = h/L$ remains constant during the cloud run. We then obtain: $k_s = E(1-4k^2)/\sqrt{k}$, where E denotes the elliptic integral function. Similarly, we can also express the volume V (per unit width) as: $V = \kappa hL$, where κ is another shape factor for a half ellipse. Here we have: $\kappa = \pi/4$. We also need to introduce an overall Richardson number, defined here by: $Ri = g'h\cos\theta/u^2$, where g' denotes the reduced gravity $g' = g\Delta\bar{\varrho}/\varrho_a$ and $\Delta\bar{\varrho} = \bar{\varrho} - \varrho_a$ is the buoyant density [Turner 1973].

The variations in the cloud mass result from entrainment of the surrounding air and entrainment/deposition of particles. During a small time increment δt, the cloud volume V has increased by a quantity δV mainly as a result of the air entrainment, thus the corresponding increase in the cloud mass is $\varrho_a\delta V$. In extreme conditions, the top layers of the snowcover are made up of new snow of weak cohesion, which can be easily entrained. Therefore we can consider that, when the front has travelled a distance

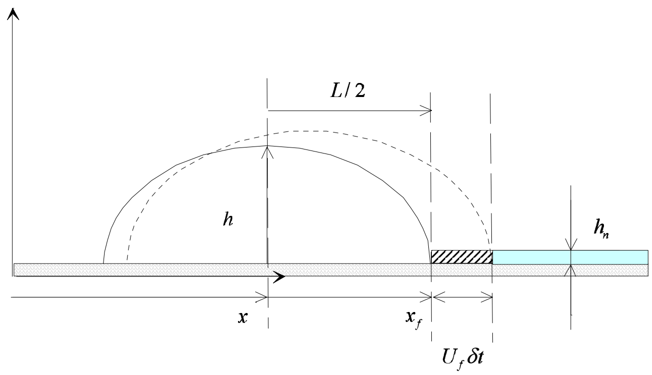

Fig. 5. Sketch of the physical system studied here.

$U_f \delta t$, where U_f is the front velocity, the top layer of depth h_n and density ϱ_s is entirely entrained into the cloud. The resulting mass variation (per unit width) writes: $\varrho_s U_f h_n \delta t$. In the same time, particles settle with a velocity v_s. During the time step δt, all the particles contained in the volume $L v_s \delta t$ deposit. Finally, by taking the limit $\delta t \to 0$, we can express the mass balance equation in the following:

$$\frac{\mathrm{d}m}{\mathrm{d}t} = \varrho_a \frac{\mathrm{d}V}{\mathrm{d}t} + \varrho_s U_f h_n - \phi \varrho_s L v_s$$

where $m = \bar{\varrho} V$ is the cloud mass. Usually the settling velocity is very low compared to the mean forward velocity of the front so that it is possible to neglect the third term in the right-hand side of the equation above. Another usual assumption is to consider that the inflow rate is proportional to a characteristic velocity (generally the mean velocity) and the surface area [Turner 1986]. Such an assumption leads to $\dot{V} = \alpha(\theta) S U$, where $\alpha(\theta)$, which is an *entrainment coefficient* depending on the inclination θ only. This assumption needs further explanations. It is usually stated that the entrainment coefficient is a function of the Richardson number. Here the overall Richardson number reflects the stabilizing effect of the density difference and the relative importance of buoyancy [Turner 1973]. In the case of a gravity current with constant supply, it is observed that for a given slope, the mean velocity U reaches a constant value, insensitive to slope but depending on the buoyancy flux (per unit width) $A = g' h U$: $U \propto \sqrt[3]{A}$ [Turner 1973; Britter & Linden 1980]. This also means that the flow adjusts rapidly to a constant Richardson number (for a given slope). In this case, using approximate equations for the mass and momentum balances (respectively $\mathrm{d}(HU)/\mathrm{d}x = \alpha U$ and

$\mathrm{d}(HU^2)/\mathrm{d}x = g'h\sin\theta$), we easily deduce that the entrainment coefficient α is a function of the Richardson number and slope: $\alpha = Ri\tan\theta$ [Turner 1973]. Here, although buoyancy supply is not constant, we assume that the entrainment coefficient α depends only on the slope. Using the simple rule $\mathrm{d}()/\mathrm{d}t = U\mathrm{d}()/\mathrm{d}x$, we obtain that the volume must linearly increase with the mass-center position x: $\mathrm{d}V/\mathrm{d}x = \alpha(\theta)S$, or equivalently: $\mathrm{d}V/\mathrm{d}x = \alpha_v\sqrt{V}$ with $\alpha_v = \alpha k_s/\sqrt{k}$. This also implies that the cloud height and length vary linearly with x. After simple algebraic manipulations, we find:

$$\frac{\mathrm{d}L}{\mathrm{d}x} = \alpha_L \tag{1}$$

$$\frac{\mathrm{d}h}{\mathrm{d}x} = \alpha_h \tag{2}$$

where $\alpha_L = \alpha_v/(2\sqrt{k\kappa})$ and $\alpha_h = \sqrt{k/\kappa}\alpha_v/2$. The final expression of the mass balance equation is:

$$\frac{\mathrm{d}\Delta\bar{\varrho}V}{\mathrm{d}t} = \varrho_s U_f h_n \tag{3}$$

The velocity of the front is given by:

$$U_f = \frac{\mathrm{d}}{\mathrm{d}t}(x_f - x + x) = U + \frac{1}{2}\frac{\mathrm{d}}{\mathrm{d}t}L = U\left(1 + \frac{\alpha_L}{2}\right)$$

The mass balance equation can also be cast in the following form, where $\Delta\bar{\varrho}$ is the variable:

$$\frac{\mathrm{d}\Delta\bar{\varrho}}{\mathrm{d}x} = \frac{1}{k}\left(1 + \frac{\alpha_L}{2}\right)\frac{h_n}{L}\frac{\varrho_s}{L} - 2\alpha_L\frac{\Delta\bar{\varrho}}{L}$$

This equation can easily be integrated. We use the following initial conditions: at $x = x_0$ and $t = 0$, we have $U = U_0$, $h = h_0$, $L = L_0$, $V_0 = \kappa h_0 L_0$, and $\bar{\varrho} = \bar{\varrho}_0$. Further assuming that the erodible snowcover thickness is constant, we obtain:

$$V(x) = \left(\sqrt{V_0} + \frac{\alpha_v}{2}(x - x_0)\right)^2$$

$$V(x)\Delta\bar{\varrho} = \varrho_s\left(1 + \frac{\alpha_L}{2}\right)h_n(x - x_0) + \Delta\bar{\varrho}_0 V_0$$

Under these assumptions, the volume and bulk density variations are only controlled by air and snow entrainments at the interface and are independent of the momentum equation. The volume rises quadratically with the downstream distance. The buoyant density $\Delta\bar{\varrho}$ first increases with the downstream distance provided that $\Delta\bar{\varrho}_s h_n > \alpha_v \Delta\bar{\varrho}_0 \sqrt{V_0}$. Then, at a critical distance $x_c - x_0 = 2\sqrt{V_0}/\alpha_v - 2V_0\Delta\bar{\varrho}_0/(h_n\varrho_s)$, the buoyant density starts decreasing slowly. At long times, we obtain the following asymptotic variation: $\Delta\bar{\varrho} \propto 4h_n\varrho_s\alpha_v^{-2}x^{-1}$. As expected, the effect of snow entrainment is to offset the cloud dilution resulting from air entrainment. At early times, snow entrainment is the prevailing mechanism leading to an increase in the buoyant density. At long times, despite snow entrainment, the cloud dilutes but snow entrainment still plays a role by controlling the decrease rate. Without snow entrainment, the cloud dilutes more quickly: $\Delta\bar{\varrho} \propto 4V_0\varrho_0\alpha_v^{-2}x^{-2}$ instead of $\Delta\bar{\varrho} \propto x^{-1}$.

Let us now examine the velocity variation. The ambient fluid exerts two types of pressure on the cloud: a term analogous to a static pressure (Archimede's theorem), equal to $\varrho_a Vg$, and a dynamic pressure. As a first approximation, the latter term can be evaluated by considering the ambient fluid as an inviscid fluid in a irrotational flow. On the basis of this approximation, it can be shown that the force exerted by the surrounding fluid on the half cylinder is $F_{\rm dyn} = \varrho_a V k_v \mathrm{d}(U)/\mathrm{d}t$, where $k_v = 2k$ is sometimes called the *added mass coefficient* [Batchelor 1967]; since at the same time the volume V varies, we finally take: $F_{\rm dyn} = \varrho_a k_v \mathrm{d}(UV)/\mathrm{d}t$. The bottom exerts a frictional force that we assume to be of Chézy form: $C_d\bar{\varrho}U^2L$ where C_d is the Chézy friction factor. Thus the momentum balance equation can be written as:

$$\frac{\mathrm{d}\bar{\varrho}VU}{\mathrm{d}t} = \bar{\varrho}gV\sin\theta - \varrho_a gV\sin\theta - k_v\varrho_a\frac{\mathrm{d}VU}{\mathrm{d}t} - C_d\bar{\varrho}U^2L \qquad (4)$$

or when the basal friction force can be neglected:

$$\frac{\mathrm{d}(\bar{\varrho} + k_v\varrho_a)VU}{\mathrm{d}t} = \Delta\bar{\varrho}gV\sin\theta$$

It is easy (but algebraically intensive) to integrate this equation. The final expression being complicated, we only provide the asymptotic expression at early and long times. To simplify the analytical expressions, here we take without loss of generality: $U_0 = 0$ and $x_0 = 0$. At early times, the velocity is independent of the entrainment parameters:

$$U \propto \sqrt{2gx\sin\theta\frac{\Delta\varrho_0}{\Delta\varrho_0 + (1+k_v)\varrho_a}} \approx \sqrt{2gx\sin\theta} \qquad (5)$$

This implies that the avalanche accelerates vigorously in the first instants ($\mathrm{d}U/\mathrm{d}x \to \infty$ at $x = 0$), then its velocity grows more slowly. At long times for an infinite plane, the velocity reaches a constant asymptotic velocity which depends mainly on the entrainment conditions:

$$U_\infty \propto \sqrt{g h_n \sin\theta \frac{(2+\alpha_L)\Delta\varrho_0}{\alpha_v(1+k_v)\varrho_a}} \tag{6}$$

Due to the slow growth of the velocity, this asymptotic velocity is reached only at very long times. Without snow entrainment, the velocity reaches a maximum at approximately $x_m^2 = (2\varrho_0/3\varrho_a)\alpha_v^{-2}V_0/(1+k_v)$:

$$U_m^2 \approx \frac{4}{\sqrt{3}}\sqrt{\frac{\varrho_0}{\varrho_a}\frac{g\sqrt{V_0}\sin\theta}{\alpha_v\sqrt{1+k_v}}}$$

then it decreases asymptotically as:

$$U \propto \sqrt{\frac{8\Delta\varrho_0}{3\varrho_a}\frac{gV_0\sin\theta}{x}\frac{1}{\alpha_v^2(1+k_v)}} \tag{7}$$

In this case, the front position varies with time as:

$$x_f \propto (g_0' V_0 \sin\theta)^{1/3} t^{2/3} \tag{8}$$

These simple calculations show the large influence of the snow entrainment on the powder-snow avalanche dynamics. In absence of snow entrainment from snowcover, the air entrainment has a key role since it directly affects the value of the maximum velocity that an avalanche can reach.

3.2 Value of the parameters

Beghin performed a large number of experiments in various conditions to obtain the values of most parameters involved in this model; the values of a few parameters (C_d, k_v) are merely assumed. Table 1 summarizes the average values that he obtained. Similar results were obtained in subsequent experiments we performed with glass beads and sawdust. In Table 1, α_w denotes the growth rate of the avalanche width for an unconfined slope. In the laboratory experiments, it is easier to measure the front position x_f and therefore the growth rate of the cloud dimensions is usually computed with respect to x_f. There is a simple relationship between either growth rates:

$$\tilde{\alpha}_h = \frac{\mathrm{d}h}{\mathrm{d}x_f} = \frac{\mathrm{d}h}{\mathrm{d}x}\frac{\mathrm{d}x}{\mathrm{d}x_f} = \frac{\alpha_h}{1+\frac{\alpha_L}{2}}$$

Similarly, we have: $\tilde{\alpha}_L = \alpha_L(1+\alpha_L/2)^{-1}$ and $\tilde{\alpha}_w = \alpha_w(1+\alpha_L/2)^{-1}$. It is worth mentioning that the mismatch between experimental data obtained by different authors can be merely due to a confusion in the definition of the growth rate. For instance, the difference between the height rates obtained by Beghin *et al.* (1981) and Akiyama and Ura (1999) comes close to zero if one takes care to this problem. Further experiments have also been conducted by Fukushima and Hayakawa (1995), and Fukushima (1998). For three-dimensional clouds, these authors proposed $\alpha_L = 0.354(\tan\theta)^{0.264}$, $\alpha_H = 2\times 10^{-3}\theta$, $k_s = \pi/4$, $k_v = 2/(8.09\sqrt[3]{\theta})$. For two-dimensional clouds, they obtained: $\kappa = \pi/4$, $\alpha_H = 2.10^{-3}\theta$, $k_s = \pi\sqrt{1+4k^2}/(2^{3/2}\sqrt{k})$, $k = 8.47/\sqrt[3]{\theta}$, $k_v = 2k$.

	2D	3D
κ (theoretical value)	$\pi/4$	$\pi/6$
κ (measured value)	0.78–0.86	–
k_v	$2k$	$1.6k$
k_s (theoretical value)	$E(1-4k^2)/\sqrt{k}$	$3/4$
k_s (measured value)	$2.15+(1.2+0.07\theta)^{-2}$	–
k	$0.16+0.04\sqrt{\theta}$	–
$\tilde{\alpha}_h$ with $h_n=0$	$3.6\times10^{-3}(\theta+11)$	$2.5\times10^{-3}(\theta+10)$
$\tilde{\alpha}_h$ with $h_n>0$	$1.7\times10^{-3}(\theta+24)$	0.08 at $\theta=30°$
$\tilde{\alpha}_L$ with $h_n=0$	$4.4\times10^{-3}(\theta+59)$	$2.1\times10^{-3}(\theta+150)$
$\tilde{\alpha}_L$ with $h_n>0$	0.45 at $\theta=42°$	0.35 at $\theta=30°$
$\tilde{\alpha}_w$ with $h_n=0$	0	0.45
$\tilde{\alpha}_w$ with $h_n>0$	0	0.4

Table 1. Values of the coefficients κ, k_v, k_s, $\tilde{\alpha}_h$, $\tilde{\alpha}_L$, $\tilde{\alpha}_w$, and C_d depending on the flow geometry (two- or three-dimensional flow) and snow entrainment. All these coefficients are dimensionless; θ is expressed in degrees. For three-dimensional clouds entraining particles from the bed, experiments were performed for a single slope ($\theta = 30°$). The length growth rate holds only for slopes in excess of 10° (below this value, the cloud is followed by a dilute tail, which makes it difficult to measure the length accurately). Data scattering is pronounced for highest slopes ($\theta > 50°$). The symbol – means that no experiment was made.

3.3 Calculation of the impact pressure

A key problem in the engineering application concerns the computation of impact pressure against an obstacle. Following Hopfinger *et al.* (1978), Beghin and Closet (1990) have suggested that the pressure distribution within the cloud can be approximated by: $P_{dyn} = \frac{1}{2}K(z)\bar{\varrho}U_f^2$ where $K(z)$ is a dimensionless coefficient reflecting the velocity variations inside the cloud. Typically, $K = 10$ for $z \leq 0.1h$, $K = 19 - 90z$ for $0.1 \leq z \leq 0.2h$, and $K = 1$ for $z \geq 0.2h$. Beghin and Closet deduced that the impact pressure must depend on the obstacle height. To evaluate this pressure, they carried out a number of laboratory experiments by examining how an obstacle of varying height modified the front motion. Their results are tabulated in Table 2 as a function of the reference pressure $p_{ref} = \frac{1}{2}\bar{\varrho}U_f^2$ and for different values of the ratio h_o/h where h_o is the obstacle height.

h_o/h	Impact pressure
0.15	$(2.5 - 40z)p_{ref}$ when $z/h < 0.05$ $\frac{1}{2}p_{ref}$ when $z/h \geq 0.05$
0.225	$0.36p_{ref}$ for $0 \leq z \leq h_0$
0.3	$0.30p_{ref}$ for $0 \leq z \leq h_0$
0.375	$0.22p_{ref}$ for $0 \leq z \leq h_0$
0.45	$0.13p_{ref}$ for $0 \leq z \leq h_0$
0.6	$0.07p_{ref}$ for $0 \leq z \leq h_0$

Table 2. Impact pressure exerted by a cloud against a wall of height h_o.

3.4 Use in engineering applications

In its original formulation, Beghin's model belongs to the family of mass-center models (like Voellmy's model). In engineering applications, since one is mainly interested in determining what happens close to the front, one has to reformulate the equations of motion in terms of the front position. In applications, we have to consider that the path slope and the thickness of the snow layer prone to be entrained vary with the downstream distance. In the following, we assume that the path profile can be described by a smooth and gently varying curve in the form $y = f(x)$, where y is the elevation and x is an arbitrary distance measured along a horizontal axis. The front position is now given by its curvilinear abscissa $s_f = \int_0^x \sqrt{1 + f'^2(x)}\mathrm{d}x$ taken from an arbitrary origin point; to first order, we have: $x \approx s_f \cos\bar{\theta}$, with $\bar{\theta}$ the mean path inclination. If the curvature radius $((1+f'^2(x))^{3/2}/f''(x))$ is large, then all happens locally as if the path were an infinite plane inclined at an angle $\tan\theta(x) = f'(x)$ with respect to the horizontal. Then, using the relationship $U = (1 - \frac{1}{2}\tilde{\alpha})U_f$ together with Eqs (1–4), we deduce the equations of motion for a two-dimensional cloud:

$$\frac{\mathrm{d}h}{\mathrm{d}s_f} = \tilde{\alpha}_h(\theta) \tag{9}$$

$$\frac{\mathrm{d}L}{\mathrm{d}s_f} = \tilde{\alpha}_L(\theta) \tag{10}$$

$$\frac{\mathrm{d}\Delta\bar{\varrho}V}{\mathrm{d}s_f} = \varrho_s h_s(s_f) \tag{11}$$

$$U_f \frac{\mathrm{d}(\bar{\varrho} + k_v \varrho_a)VU_f}{\mathrm{d}s_f} = \frac{\Delta\bar{\varrho}gV\sin\theta}{1 - \frac{1}{2}\tilde{\alpha}} - C_d L \left(1 - \frac{1}{2}\tilde{\alpha}\right)\varrho U_f^2 \tag{12}$$

Such a system of ordinary differential equations can easily be integrated numerically.

3.5 Comments

In the theoretical development of his model, Beghin used Turner's approximation for the inflow rate at the boundary between the cloud and the surrounding fluid. This approximation implies that the cloud growth rate is independent of the snow entrainment. This result contrasts with experimental measurements and field data. In his laboratory experiments, Beghin found for a two-dimensional cloud over a 42° slope: $\tilde{\alpha}_h = 0.11$ for a cloud entraining particles against $\tilde{\alpha}_h = 0.19$ when there is no particle entrainment. When taking a closer look at video tapes of real events, one observes that, insofar as the front incorporates snow, the height grow rate is close to zero. Figure 6 shows a sequence of three photographs of a powder snow avalanche in the Raffort site (Méribel-les-Allues, France) on 21 January 1981. The avalanche was artificially triggered after heavy snow falls[1] (210 cm within 7 days). In the first two photographs, it is seen that the height is a few meters high (the height is approximately twice the roof height of the chalets). When the front passes the chalets, built over a gentle slope, there is a significant growth of the head. Another point merits being mentioned: in the first instants, the airborne has a sharp front while when it reaches the chalets, the front structure presents several fingers, which a steep nose and a smoother boundary.

[1] From 13 to 20 January 1981, the French Alps underwent one of the worst snowstorms over the last thirty years, with an intense and destructive avalanche activity in the northern French Alps.

Using field data from the Ryggfonn site (Norway), Nishimura *et al.* (1995) have also noticed a significant mismatch between field data and Beghin's values. They have computed the height and width growth rates as a function of slope. It clearly appears that: (i) Beghin's value of width growth rate is correct only when the avalanche runs out, (ii) during the release and flow phases, the width is fairly constant (although the slope is open), (iii) the height growth rate is close to zero for steep slopes ($\theta > 25°$), (iv) for $\theta \leq 25°$, it is in the range $0.19 - 0.22$ while Beghin's values vary in the range $0.02 - 0.08$.

These observations have two important implications. First, from a theoretical viewpoint, the dependency of the growth rates on the path slope results from the approximation of a constant overall Richardson number; such an approximation holds for a gravity current for a constant buoyancy supply but fails probably in the present case, where there are substantial variations in the buoyancy supply. Second, from a practical point of view, the fact that in Beghin's model, the growth rates depend on the snow entrainment is a consequence of the parameter fitting and not a theoretical prediction; moreover the values obtained by Beghin from laboratory experiments are much larger than field values. When applying Beghin's model to real cases, a strategy is to reduce the width and height growth rates to obtain more realistic predictions of the cloud height.

Another point in Beghin's model merits further discussions. Though its engineering version involves the front position and velocity, Beghin's model belongs to the class of mass center models. This means that all spatial processes occurring in the front, tail, and body, are averaged and replaced by an overall effective process. A different viewpoint has been expressed by Simpson and Huppert in the context of gravity currents (for a good introduction, see [Hogg *et al.* 2000]): the motion of a gravity current is mainly controlled by the front. Using the von Kármán–Benjamin boundary condition at the leading edge – stating that the front motion is characterized by a constant *Froude number* $Fr = U/\sqrt{gh}$, i.e. $Fr^2 = g'/(g\,Ri)$ –, Huppert and Simpson (1980) developed a very simple model called the "box model". They considered a two-dimensional gravity current as a series of equal cross-sectional area rectangles (of length $l(t)$ and height $h(t)$) advancing over a horizontal surface: $u = Fr\sqrt{g'h}$ and $V(t) = h(t)l(t) = V_0$ where V_0 denotes the initial volume (per unit width) of fluid (here $Fr = \sqrt{2}$ inferred from theoretical considerations using the Bernoulli equation). Using $u = \mathrm{d}l/\mathrm{d}t$ and integrating the volume equation

Fig. 6. Avalanche in the Raffort path (Méribel-les-Allues, Savoie) on 21 January 1981. Courtesy of Méribel Alpina.

leads to:

$$l(t) = \left(\frac{3}{2}Fr\right)^{2/3} (g'V_0)^{1/3} t^{2/3} \quad (13)$$

Comparison of (8) and (13) reveals the same asymptotic behaviour, except that in Beghin's model, the position depends on the inclination θ. Many experiments have been performed on the motion of a two-dimensional cloud over horizontal surfaces and have demonstrated the reliability of the box model. Though a direct comparison of the predictions provided by the two model is not possible insofar as the box model approach only treats horizontal flow surfaces, one can wonder whether a box model would not be more appropriate for describing particle clouds entraining particles from the bed.

4 Application to the site of La Sionne

There are very few powder snow avalanche events that have been documented accurately and thoroughly. This made it very difficult to test the efficiency of Beghin's model. In the course of February 1999, three powder snow avalanches were triggered and monitored in the Sionne site (Switzerland, Wallis). This series constitutes an outstanding source of information.

The site is located above Sion (Rhone valley). The path extends in the south-east facing slope of Crêta Besse between approximately 2550 (2400–2700 m) and 1450 m in elevation and its length exceeds 2.2 km. The bottom point of the path is marked by the Sionne river. Flowing avalanches can be confined in the river bed and continue to flow. On the whole, the path is open, except between 1800 and 2000 m a.s.l, where avalanches are confined in one or two gullies. The overall slope is high (52%); the path slope decreases rather regularly between the release zone (slope: 80%) and the run-out zone (mean slope close to 30%). More information can be found in the report edited by Issler (1999) and the article by Ammann (1999). The reader is also referred to recent papers concerning the events of February 1999 [Dufour *et et al.* 2001, Schaer & Issler 2001, Vallet *et al.* 2001].

Here, we only examine the avalanche of 10$^{\text{th}}$ February 1999, for which the front velocity was recorded and the variations in impact pressure with time were measured on a tubular mast and a wedge located at the elevation of 1640 m. In Fig. 7, we have reported the variation in the mean front velocity U_f as a function of the downstream distance s_f: the black boxes correspond to the measured data while the solid line represents the solution obtained by integrating Eqs (9–12) numerically and the dashed line corresponds to the variations in the asymptotic velocity [given by Eq. (6)]. In either case, we have considered a two-dimensional cloud. For the model parameters, we have taken the values obtained by Beghin and tabulated in Table 1. For the initial conditions, on the basis of the photogrammetric study by Vallet *et al.* (2001), we have considered that on average, the released snow layer h_s is 1 m thick.

Fig. 7. Variation of the front velocity with the downstream distance. Initial conditions: $V_0 = 100$ m^2, $U_0 = 0$ m/s, $\varrho_0 = 100$ kg/m^3, $h_0 = 1$ m, $L_0 = 100$ m; $h_s = 1$ m when $y \geq 2200$ a.s.l., $h_s = 0$ for $y \leq 1900$ a.s.l., inbetween we have assumed (somewhat arbitrarily) a quadratic dependence of h_s on the elevation y; $\varrho_0 = 150$ kg/m^3. Parameters: $k = 0.36$, $\alpha_v \approx 0.255$, $\alpha_h = 0.085$, $\alpha_h = 0.245$, $\kappa = Pi/4$. Black boxes: front velocity measurements (Courtesy of François Dufour and EISLF). Continuous curves: numerical solution to the equations of motion (9–12). Dashed curve: asymptotic velocity (given in part by Eq. 6 in which x has been replaced by s_f and θ by $\arctan|f'(x)|$ where $f(x)$ is the interpolating function of the path profile); same conditions as for the numerical solution except that $h_s = 1$ over the entire path.

Comparing numerical results obtained using Beghin's model and field data reveals a good agreement. On the contrary, assuming no snow entrainment leads to a very different result as shown in Fig. 8: in the early times, the curves with and without snow entrainment coincide but rapidly the curve corresponding to the no-entrainment solution decays while the curve pertaining to the entrainment solutions still grows. In Fig. 7, there is no much difference between the numerical solution and the theoretical approximation (asymptotic velocity). This demonstrates that the velocity reaches its asymptotic state fairly quickly and that the initial conditions do not significantly influence the subsequent evolution of the front velocity.

Fig. 8. Variation of the asymptotic front velocity with the downstream distance. Continuous curve: solution with snow entrainment. Dashed curve: solution without snow entrainment. Same flow conditions as for Fig. 7.

Figure 9 shows the variation in the reference pressure. The pressure peak is found close to 12 kPa while the reference pressure at the tubular mast is approximately 6 kPa. Even if we multiply this reference pressure by 10 (see Sec. 3.3), the computed value differs substantially from the range of measured values. Issler and Schaer (2001) have found that, on average, the pressure exerted by the avalanche of 10$^{\text{th}}$ February 1999 on the mast (at 3.9 m from the ground) was close to 400 kPa. Instantaneous peaks exceeding 1200 kPa were also measured. The damage to the measurement structures confirmed that very high levels of pressure were attained in the three avalanches of February 1999.

Here we have not reported the variation in the cloud height h since it varies almost linearly with downstream distance. Close to the measurement structures, the computed value of h is approximately 180 m while, according to Issler and Schaer (2001), the cloud height did not exceed 50 m for the avalanche of 10$^{\text{th}}$ February 1999. This is an important clue which reveals that the cloud growth rates measured in the laboratory are approximately 3 to 4 times higher than the rates pertaining to real avalanches. If we assume that the true volume growth rate is $\alpha_v = 0.255/3 \approx 0.08$, we find that at $y = 1640$ a.s.l, the front velocity is 64 m/s (in fairly good agreement with field observations), the bulk density is $\bar{\varrho} = 52\,kg/m^3$, and the reference pressure is 120 kPa; therefore applying a multiplying factor as explained in Sec. 3.3, we found a maximum pressure of 1200 kPa, which is consistent with the field data. Furthermore, sensibility tests show that the reference pressure is much less influenced by other model parameters such as h_s. The value of the entrainment coefficient α_v is thus found to be a key parameter in the powder snow avalanche dynamics.

Fig. 9. Variation of the reference pressure with the downstream distance. Same flow conditions as for Fig. 7. Continuous curve: numerical solution to Eqs. (9–12) with $\alpha_v = 0.255$. Dashed curve: approximate solution with $\alpha_v = 0.085$.

5 Concluding Remarks

This article has been the opportunity to present the different developments of Beghin's model from 1981 to nowadays. Despite its apparent simplicity, this model can be used to correctly describe various flow conditions (particle cloud with or without entrainment, two- or three-dimensional flow). For laboratory experiments, its success is tightly related to the adjustment of growth rate parameters, which can be easily performed. When applying this model to real cases, so far the only solution at our disposal has been to use the parameters fitted on laboratory experiments. Interestingly enough, the predictions of the front velocity obtained in this way are in good agreement with the few field data. In contrast, the computed cloud height differs by a factor 3 to 4 from the measured value and the maximum impact pressure is 200 times smaller than the measured pressure peak. A better agreement can be obtained as soon as the entrainment coefficient α_v (volume growth rate) is changed.

Snow entrainment has been taken into account in a simple way in Beghin's model: it is merely assumed that the entire layer of newly fallen snow can be incorporated into the cloud by the front. Snow entrainment is a key process in the avalanche dynamics, which dictates the damage potential of the avalanche. According to Beghin's model the maximum velocity reached by the avalanche is slightly modified by snow entrainment but, since snow entrainment balances the cloud dilution resulting from air entrainment, the avalanche can maintain very high velocities over long distances whereas, if there is no snow entrainment, the avalanche velocity decays rapidly. Another effect of snow entrainment is indirectly described in Beghin's model: snow entrainment involves a lower volume growth rate α_v. This makes it possible to achieve high values of bulk density and thus of impact pressure. A proper evaluation of the entrainment coefficient (function of snow entrainment) is needed for Beghin's model to be applicable to real cases. The present study leads to estimates of α_v which are three times smaller than those previously obtained in the laboratory.

Acknowledgment

This work is dedicated to the memory of Philippe Revol and Pierre Beghin, who were responsible for all the developments in the model. Both disappeared tragically without publishing their works. The article is a summary of internal reports written by Beghin and Revol in the last two decades. I am grateful to the Institut National of Sciences de l'Univers for providing financial support and the French Ministère de la Recherche for providing a grant for the thesis of Marie Clément. Experiments were performed by Pierre Beghin, Frédéric Ousset, Christian Edmond-Gris, Philippe Revol, Hervé Bellot, Marie Clément, and Rémi Magnard. Specific thanks to François Dufour who kindly received us in his site and provided data.

References

1. Akiyama, J. and Ura, M., "Motion of 2D buoyant clouds downslope", *Journal of Hydraulic Engineering*, **125** (1999) 474–480.
2. Ammann, W.J.,"A new Swiss test-site for avalanche experiments in the Valleée de la Sionne", *Cold Region and Science Technology* , **30** (1999) 3–11.

3. Bozhinskiy, N. and Losev, K.S., *The fundamentals of Avalanche Science*, translated from Russian by C.E. Bartelt, Communication 55 (EISFL, Davos, 1998).
4. Batchelor, G.K., "An introduction to fluid dynamics" (Cambridge University Press, 1967) 614.
5. Beghin, P. and Brugnot, G., "Contribution of theoretical and experimental results to powder-snow avalanche dynamics", *Cold Review Science and Technology*, **8** (1983) 63–73.
6. Beghin, P. and Closet, J.-F., "Effet d'une digue sur l'écoulement d'une avalanche poudreuse", *Informations Techniques du Cemagref* **77/3** (Cemagref, 1990) 8 p. (In French.)
7. Beghin, P., "Etude du phénomène de reprise", Internal report (Cemagref, 1990) 23 p. (In French.)
8. Beghin, P., Hopfinger, E.J. and Britter, R.E., "Gravitational convection from instantaneous sources on inclined boundaries", *Journal of Fluid Mechanics*, **107** (1981) 407–422.
9. Beghin, P. and Olagne, X., "Experimental and theoretical study of the dynamics of powder snow avalanches", *Cold Regions Science and Technology*, **19** (1991) 317-326.
10. Britter, R.E., Simpson, J.E., "Experiments on the dynamics of a gravity current head", *Journal of Fluid Mechanics* **88** (1978) 223–240.
11. Britter, R.E. and Linden, P.F., "The motion of the front of a gravity current travelling down an incline", *Journal of Fluid Mechanics*, **99** (1980) 531–543.
12. Capart, H. and Young, D.L., "Formation of a jump by the dam-break wave over a granular bed", *Journal of Fluid Mechanics*, **32** (1998) 121–135.
13. Dufour, F., Gruber, U, Ammann, W.J., "Sur la piste des avalanches catastrophes" (in French), *Les Alpes* **2** (2001) 9–15; Dufour, F., Bartelt, P, Ammann, W.J., "Overview of the 1999 measurements at the SLF test site Vallé de la Sionne " [unpublished] (2001) 7 p; see also "Messungen in Vallée de la Sionne", in *Der Lawinenwinter 1999*, edited by W. Ammann (EISFL, Davos, 2000) pp. 353–356 (in German).
14. Ellison, T.H. and Turner, J.S., "Turbulent entrainment in stratified flows", *Journal of Fluid Mechanics*, **6** (1959) 423–448.
15. Escudier, M.P. and Maxworthy, T., "On the motion of turbulent thermals", *Journal of Fluid Mechanics*, **61** (1973) 541-552.
16. Evans, S.G., "The field documentation of highly mobile rock and debris avalanches in the Canadian Cordillera" in *international workshop on rapid gravitational mass movements* edited by L. Buisson (Cemagref, Grenoble, 1993) 73–76.
17. Fraccarollo, L. and Capart, H., "Riemann wave description of erosional dam break flows", *Journal of Fluid Mechanics*, **461** (2002) 183–228.
18. Fukushima, Y. and Parker, G., "Numerical simulation of powder-snow avalanches", *Journal of Glaciology*, **36** (1990) 229–237.
19. Fukushima, Y. and Hayakawa, N., "Dynamics of three-dimensional inclined thermal", *Journal of Hydraulic Engineering*, **121** (1995) 600-607.
20. Fukushima, Y., "Numerical simulation of gravity current front", *Journal of Hydraulic Engineering*, **124** (1998) 572-578.
21. Garcia, M.H., "Depositing and eroding sediment-driven flows: turbidity currents", Ph.D Thesis (University of Minnesota, Minneapolis, 1990) 179 p.
22. Garcia, M. and Parker, G., "Entrainment of bed sediment into suspension", *Journal of Hydraulic Engineering*, **117** (1991) 414–435.

23. Hermann, F., Issler, D. and Keller, S., "Numerical simulations of powder-snow avalanches and laboratory experiments in turbidity currents" in *International Workshop on Gravitational Mass Movements* edited by L. Buisson (Cemagref, Grenoble, 1993) 137–144.
24. Hogg, A.J., Ungarish, M., and Huppert, H.E., "" Particle-driven gravity currents: asymptotic and box models solutions", *European Journal of Mechanics* ser. B **19** (2000) 139–165.
25. Hopfinger, E.J. and Tochon-Danguy, J.-C., "A model study of powder-snow avalanches", *Journal of Glaciology*, **81** (1977) 343–356.
26. Hopfinger, E.J., Layat, S, and Roche, J.-P., "Mesures des pressions dynamiques", appendice to the article "Effets de la densité et de la pente sur la dynamique des avalanches poudreuses" by P. Beghin and E.J. Hopfinger, in *2nd International Meeting Snow and Avalanches*, edited by the Association Nationale d'Etudes de la Neige et des Avalanches (Grenoble, 1978) 183–187.
27. Huppert, H.E. and Simpson, J.E., "The slumping of gravity currents", *Journal of Fluid Mechanics*, **99** (1980) 785–799.
28. Huppert, H.E., "Quantitative modelling of granular suspensions flows", *Philosophical Transactions of the Royal Society of London* ser. A **356** (1998) 2471–2496.
29. Hutter, K., "Avalanche dynamics" in *Hydrology of Disasters*, edited by Singh, V.P. (Kluwer Academic Publications, Dordrecht, 1996) 317-392.
30. Issler, D., (Ed.), *European Avalanche Test Sites*, Communication 55 (EISFL, Davos, 1998).
31. Issler, D., "Modelling of snow entrainment and deposition in powder-snow avalanches", *Annals of Glaciology*, **26** (1998) 253–258.
32. Kulikovkiy, A.G. and Svehnikova, E.I., "Model dlja rascheta dvizhija pilevoi snezhnoi lavini (a model for computing powdered snow avalanche motion) [in Russian]", *Materiali Glatsiologicheskih Issledovanii (Data of Glaciological Studies]*, **31** (1977) 74–80; translated in French by G. Brugnot; see also Eglit, M.E. and Revol, P., "Models for powder snow avalanches: comparison of two approaches", in *25 years of snow avalanche research* edited by Hestnes, E. (Norwegian Geotechnical Institute, Voss, 1998) 99–103.
33. Naaim, M. and Gurer, I., "Two-phase numerical model of powder avalanche. Theory and application", *Journal of Natural Hazard*, **16** (1997) 18–145.
34. Nishimura, K., Sandersen, F., Kristensen, K., and Lied, K., "Measurement of powder snow avalanche - nature", *Surveys in Geophysics* **16** (1995) 649–660.
35. Parker, G., "Conditions for the ignition of catastrophically erosive turbidity currents", *Marine Geology*, **46** (1982) 307–327.
36. Parker, G., Fukushima, Y. and Pantin, H.M., "Self-accelerating turbidity currents", *Journal of Fluid Mechanics*, **171** (1986) 145–181.
37. Parker, G., Garcia, M., Fukushima, Y., and Yu, W., "Experiments on turbidity currents over an erodible bed", *Journal of Hydraulic Research*, **25** (1987) 12–147.
38. Schaer, M, Issler, D., "Particle densities, velocities and size distribution in large avalanches from impact-sensor measurements", *Annals of Glaciology*, **32** (2001) 321–328.
39. Scheiwiller, T., Hutter, K. and Hermann, F., "Dynamics of powder snow avalanches", *Annales Geophysicae*, **5B** (1987) 569–588.
40. Simpson, J.E., "Effects of a lower boundary on the head of a gravity current", *Journal of Fluid Mechanics*, **53** (1972) 759–768.
41. Tochon-Danguy, J.-C. and Hopfinger, E.J., "Simulation of the dynamics of powder avalanches", in *International symposium on snow mechanics* (IAHS, Grindelwald, 1974) 369–380.

42. Turner, J.S., “Turbulent entrainment: the development of the entrainement assumption, and its application to geophysical flows”, *Journal of Fluid Mechanics*, **173** (1986) 431-471.
43. Turner, J.S., *Buoyancy Effects in Fluids*, (Cambridge University Press, Cambridge, 1973)
44. Vallet, J., Gruber, U., Dufour, F., “Photogrammetric avalanche volume measurements at Vallé de la Sionne, Switerland”, *Annals of Glaciology*, **32** (2001) 141–146.